Received: 19 May 2022 | Revised: 30 December 2022 | Accepted: 9 January 2023

DOI: 10.1096/fj.202200762RR

THE FASEB JOURNAL

RESEARCH ARTICLE

Loss of *Adgra3* causes obstructive azoospermia with high penetrance in male mice

Maja L. Nybo[1] | **Jone M. Kvam**[1] | **John E. Nielsen**[2] | **Hanne Frederiksen**[2] | **Katja Spiess**[1] | **Kristian H. R. Jensen**[1] | **Sarina Gadgaard**[1,3] | **Anna L. S. Walser**[1] | **Jesper S. Thomsen**[4] | **Pamela Cowin**[5,6] | **Anders Juul**[2,7] | **Martin Blomberg Jensen**[8,9] | **Mette M. Rosenkilde**[1]

[1]Laboratory for Molecular Pharmacology, Department of Biomedical Sciences, Faculty of Health and Medical Sciences, University of Copenhagen, Copenhagen, Denmark

[2]Department of Growth and Reproduction and International Center for Research and Research Training in Endocrine Disruption of Male Reproduction and Child Health (EDMaRC), Copenhagen University Hospital – Rigshospitalet, Copenhagen, Denmark

[3]Bainan Biotech, Copenhagen, Denmark

[4]Department of Biomedicine, Aarhus University, Aarhus, Denmark

[5]Department of Cell Biology, New York University School of Medicine, New York, New York, USA

[6]Department of Dermatology, New York University School of Medicine, New York, New York, USA

[7]Department of Clinical Medicine, University of Copenhagen, Copenhagen, Denmark

[8]Group of Skeletal, Mineral and Gonadal Endocrinology, Department of Growth and Reproduction, Copenhagen University Hospital – Rigshospitalet, Copenhagen, Denmark

[9]Division of Bone and Mineral Research, HSDM/HMS, Harvard University, Boston, Massachusetts, USA

Correspondence
Mette M. Rosenkilde, Laboratory for Molecular Pharmacology, Department of Biomedical Sciences, Faculty of Health and Medical Sciences, University of Copenhagen, Copenhagen, Denmark.
Email: rosenkilde@sund.ku.dk

Funding information
European Research Council, ERC, Grant/Award Number: 682549; Lundbeck Foundation, Grant/Award Number: R268-2017-409; Novo Nordisk Foundation, Grant/Award Number: NNF20OC0059475

Abstract

The adhesion receptor ADGRA3 (GPR125) is a known spermatogonial stem cell marker, but its impact on male reproduction and fertility has not been examined. Using a mouse model lacking *Adgra3* (*Adgra3*$^{-/-}$), we show that 55% of the male mice are infertile from puberty despite having normal spermatogenesis and epididymal sperm count. Instead, male mice lacking *Adgra3* exhibited decreased estrogen receptor alpha expression and transient dilation of the epididymis. Combined with an increased estradiol production, this indicates a post-pubertal hormonal imbalance and fluid retention. Dye injection revealed a blockage between the ejaculatory duct and the urethra, which is rare in mice suffering from infertility, thereby mimicking the etiologies of obstructive azoospermia found in

Abbreviations: AGD, anogenital distance; aGPCR, adhesion G protein-coupled receptor; AMH, anti-Müllarian hormone; Amhr2, anti-Müllerian hormone receptor 2; Aqp1, aquaporin-1; Aqp9, aquaporin-9; Ar, androgen receptor; BMD, bone mineral density; CA II, IV, XIV, carbonanhydrase II, IC, XIV; CBAVD, congenital bilateral absence of vas deferens; CFTR, cystic fibrosis transmembrane conductance regulator; Cyp19a1, aromatase; DEXA, dual-energy X-ray absorptiometry; ERα, estrogen receptor alpha; FSH, follicle-stimulating hormone; GAIN domain, GPCR autoproteolysis-inducing domain; HE, hematoxylin and eosin; HBD, hormone-binding domain; ID4, inhibitor of differentiation 4; Ig, immunoglobulin-like; IHC, immunohistochemistry; LRR, leucine-rich repeats; NHE3, sodium-hydrogen antiporter 3; PFA, paraformaldehyde; RT-qPCR, qualitative reverse transcript polymerase chain reaction.

and NNF17OC0029222; Valter Alex Torbjørn Eichmuller, Grant/Award Number: 2020-117043; Kirsten and Freddy Johansens Foundation, Grant/Award Number: 2017-112697; Dansk Frie Forskningsråd; Department of Defense, Grant/Award Number: W81XWH-17-1-0013 BC160959

human male infertility. To summarize, male reproductive tract development is dependent on ADGRA3 function that in concert with estrogen signaling may influence fluid handling during sperm maturation and storage.

KEYWORDS

adhesion G protein-coupled receptor, ejaculatory duct, ejaculatory duct obstruction, estrogen, GPR125, infertility, seminal vesicles, Wnt signaling

1 | INTRODUCTION

Infertility is a global health problem affecting one in seven couples worldwide,[1,2] and a male factor is responsible for up to 50% of these cases.[3,4] Although there are multiple etiologies resulting in infertility, frequent causes include impaired spermatogenesis due to genetic, developmental, or hormonal disorders, and obstruction within organs related to the male reproductive system.[5]

Spermatogenesis is a complicated process that begins with spermatogonial stem cells undergoing self-renewal inside the testis. After an intricate series of events, these cells end up as haploid spermatozoa.[5,6] Upon ejaculation, the mature sperm leave the cauda epididymis, pass through the vas deferens, and enter the ejaculatory ducts. Here, seminal vesicular and prostate secretions are mixed with sperm before the ejaculate leaves the urethra.

Sertoli cells are essential for spermatogenesis in the testis, and its function is tightly regulated by follicle-stimulating hormone (FSH) from the pituitary gland and androgens from the testicular Leydig cells, which together regulate the spermatogenesis.[7,8] In concert with estrogens and anti-Müllerian hormone (AMH), FSH and testosterone ensure appropriate development and function of the epididymis, prostate, seminal vesicles, and the connecting ducts of the male reproductive tract.[9] Due to its regulation of aquaporin-9 (AQP9),[10–12] sodium-hydrogen antiporter 3 (NHE3),[13–15] and cystic fibrosis transmembrane conductance regulator (CFTR),[16] estrogen receptor alpha (ERα) is instrumental for resorption of water in efferent ducts and epididymis and thus, a critical determinant of the epididymal microenvironment, as well as sperm maturation, storage, and passage.

Adhesion G protein-coupled receptors (aGPCRs) make up the second largest GPCR family.[17] They are characterized by a classical 7-transmembrane domain and a large extracellular segment, containing a GPCR autoproteolysis-inducing (GAIN) domain and multiple conserved adhesion domains.[18] The aGPCR family is comprised of 33 members with a wide range of biological functions, from ADGRC1 (CELSR1), required for ureteric bud development in the kidney,[19] to ADGRG2 (GPR64), which is required for male fertility.[20] Several aGPCRs show testicular expression patterns,[21] but only a few have been functionally characterized.[20,22–24]

ADGRA3 (GPR125) is an orphan member of the aGPCR family[18] with which it shares the characteristic aGPCRs domains, including the GAIN domain, multiple leucine-rich repeats (LRR), an immunoglobulin-like domain (Ig), and a hormone-binding domain (HBD) (Figure 1A).[18] ADGRA3 was initially identified as a spermatogonial stem cell marker in multiple species.[25–27] Later studies showed an increase in *Adgra3* expression within the choroid plexus after acute brain injury[28] and demonstrated an essential role of ADGRA3 in murine mammary and lacrimal gland development.[29,30] ADGRA3 internalizes constitutively,[31] recruits disheveled proteins to the membrane, and modulates the Wnt/β-catenin pathway via regulation of β-catenin transcriptional activity.[32,33] This directly links the receptor to cell orientation and planar cell polarity and suggests a role in directional outgrowth and cell migration.[29,30] Murine spermatogonial stem cells lacking the cytoplasmic domain of ADGRA3 are nevertheless able to maintain their progenitor stem cell properties.[26] Thus, as the function of the receptor in the male reproductive organs remain unknown, the aim of the presented study was to investigate the fertility and spermatogenesis in males lacking ADGRA3.

2 | MATERIALS AND METHODS

2.1 | Animals

The *Adgra3*$^{-/-}$ strain was constructed by genOway, as follows: Exons 5 and 6 of the *Adgra3* gene were flanked by *LoxP* using a Neo cassette blanked by FRT sites into a RMM1-HR targeting vector. Mice generated from these ES cells were bred to a Flp delete strain to remove the Neo cassette. The mice were subsequently bred to generate global excision of exon 5 and 6 in the germline, by crossing with ubiquitous-Cre expressing driver mice (CMV;Cre Tg, RRID:IMSR_JAX:006054; Jackson Laboratory). All experiments were conducted using male mice. Animals were homozygous or heterozygous for the mutant allele (*Adgra3*$^{-/-}$ and *Adgra3*$^{+/-}$, respectively), or homozygous

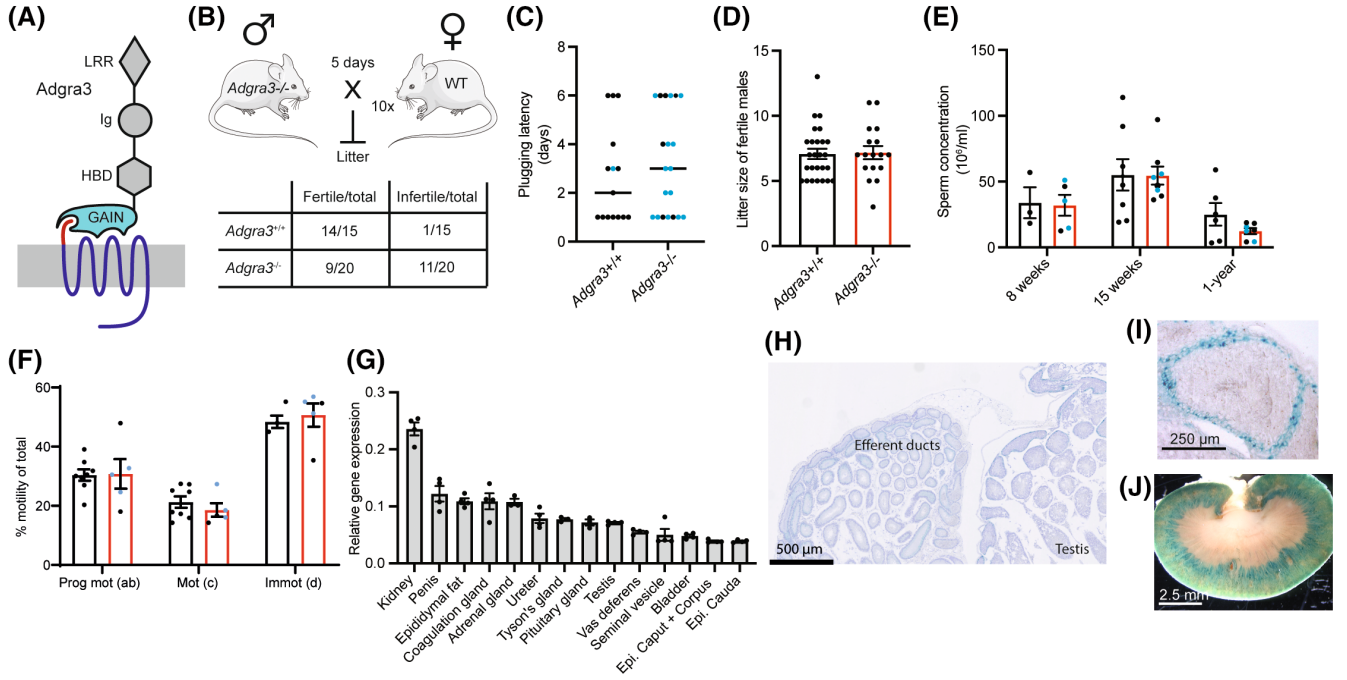

FIGURE 1 Lack of *Adgra3* in male mice causes infertility, despite normal sperm production. (A) Schematic drawing of Adgra3, containing its 7-transmembrane domain (blue), the Stachel sequence (red linker), the GPCR autoproteolysis-inducing domain (GAIN), and the three extracellular domains; hormone-binding domain (HBD), immunoglobulin domain (Ig), and leucine-rich region (LRR). (B) Fertility study setup and proportion of fertile and infertile *Adgra3*$^{+/+}$ and *Adgra3*$^{-/-}$ males based on 8 months of breeding with 10 different females. (C) Plugging latency of *Adgra3*$^{+/+}$ and *Adgra3*$^{-/-}$ males as an indication of mounting behavior. Each dot (n = 15–20) represents the period between cohabitation with females and detection of the first plug in a mated female; lines are the median; blue dots indicate infertile males. (D) Litter sizes of fertile *Adgra3*$^{+/+}$ and *Adgra3*$^{-/-}$ males (n = 17–26 individual breedings). (E) Sperm count at 8, 15 weeks, and 1 year of age (n = 5–8) taken from cauda of the epididymis. Blue dots indicate infertile males. (F) Sperm motility measured as progressive (ab), non-progressive (c) or immotile (d) sperm cells at 8 weeks of age. Blue dots indicate infertile males. (G) *Adgra3* expression pattern in 8-week-old C57BL6/J male mouse urogenital tract (n = 4). (H–J) Representative pictures of X-gal stained *Adgra3*$^{lacZ/+}$ showing epididymis and testis (H), staining of the spermatogonial stem cells within testis (I), and within the cortex of the kidney (J). In all datasets, each dot represents a single animal. Data presented as mean ± SEM. Statistics included two-tailed Student's t test (C,D,F), and two-way ANOVA with Šídák correction for multiple comparisons (E). Figures were created with smart.servier.com.

for the wild-type allele (*Adgra3*$^{+/+}$), all male mice bred from heterozygous parents. Mice were kept group-housed after weaning. All experiments and animal housing were conducted in a 12-h light/dark cycle at 22 ± 2°C, 55 ± 10% humidity with *ad libitum* access to chow (SAFE D30, SAFE diets) and tap water. Mice housing and experiments complied with institutional guidelines and approved by the Animal Experiments Inspectorate under the Danish Ministry of Food, Agriculture, and Fisheries (license numbers 2018-15-0201-01442, 2017-15-0202-00117 and 2017-15-0201-01235).

2.2 | Fertility and latency studies

Fertility and latency studies were conducted to investigate the mounting behavior and fertility of the *Adgra3*$^{-/-}$ male mice and littermate controls. Each 8-week-old male was introduced to one 8-week-old C57BL6/J female mouse (RRID:IMSR_JAX:000664; Jackson Laboratory) for 5 days. Every morning at 9 am, the female was checked for plugs to examine the mounting behavior of the male, and records were kept on the day a plug was observed. Pups were counted on the day of birthing. The experiment was repeated 10 times over 8 months, with the same male mouse and a new C57BL6/J female mouse each time.

2.3 | Anogenital distance

The anogenital distance (AGD) of male *Adgra3*$^{-/-}$ and littermate controls were measured using a photographic method, which allowed for repeated assessments. The mice were placed on a Plexiglas platform with built-in measuring tape and a camera placed approximately 10 cm underneath. The mice were held stationary by the tail, while pictures were taken. AGD was measured as the length of the perineum from the center of the

genital papilla to the proximal end of the anus,[34] and assessed by two independent investigators blinded to the genotype.

2.4 | Tissue preparation, plasma samples, and quantitative RT-PCR (RT-qPCR)

Mice were decapitated, and blood was collected in Microvette 500 K3E collection tubes (Sarstedt) from the main artery. Plasma was isolated for hormone measurements by centrifugation at 4°C for 15 min at 1000 rpm. For bone mineral density analysis, the right femur was carefully harvested, cut free of muscle tissue, fixed in ice-cold 70% ethanol, and stored at 4°C until further examination. Tissue for RT-qPCR or sperm count was snap-frozen and stored at −80°C. Tissue for histology was fixed overnight at 4°C in 3.7% paraformaldehyde (PFA) and subsequently embedded in paraffin. RNA and cDNA were prepared using RNeasy Micro Kits (Qiagen) and High-Capacity cDNA Reverse Transcription Kits (Thermo Fisher Scientific) according to the manufacturers' protocols. Subsequently, RT-qPCR was conducted using PrecisionPlus qPCR Master Mix with low ROX and SYBR Green (Primer Design). Primers were designed to specifically target each mRNA, spanning introns to eliminate genomic DNA: *36b4*_Frd TCATCCACGAGGTGTTTGACA, *36b4*_Rv GGCAACGAGGCAACAGTT; *Ywhaz*_Frd AGACGGAA GGTGCTGAGAAA, *Ywhaz*_Rv GAAGCATTGGGGAT CAAGAA; *Ar*_Frd GGACCATGTTTTACCCATCG, *Ar*_ Rv TCGTTTCTGCTGGCACATAG; *Amhr2*_Frd CACAA GTGGAGATGCAAGGA, *Amhr2*_Rv CAGAAGTCAGT GCCACAGGA; *Cyp19a1*_Frd TTCTACATTAAACCCAG TTGC, *Cyp19a1*_Rv GACTTCTTTATTTGAAATGCACC; *Esr1*_Frd CCTCCCGCCTTCTACAGGT, *Esr1*_Rv CACAC GGCACAGTAGCGAG, *Aqp9*_Frd TGGGGATTTGA GGTCTTCAC, *Aqp9*_Rv GGTTCTGCCTTCACTTCTGG; *Nhe3*_Frd CGTGGATTGTGTGAAAGGCA, *Nhe3*_Rv CAGCATCTCGGAGGTCAGAT; *CFTR*_Frd GGCCTTCA TCGCATTGGAAT, *CFTR*_Rv CCAGAGAAGCCCCA TCAGAA; *Aqp1*_Frd GATTGACTACACTGGCTGCG, *Aqp1*_Rv GGTCATACTCCTCCACCTGG; *CaII*_Frd GATAAAGCTGCGTCCAGGAGC, *CaII*_Rv CCCATATT TGGTGTTCCAGTGAA; *CaIV*_Frd CTGCTAGGACA AAGGTGAACC, *CaIV*_Rv CTCCACTGTGTGTTGAT TGTTCT; *CaXIV*_Frd GTGGGCGAGACTGAGAATCC, *CaXIV*_Rv GTTGTGAGTGAGCCGTTGTAG. All primers were diluted to a concentration of 250 nM per reaction, and cDNA to 1 ng/µl. Relative gene expression was normalized to the average of *Ywhaz* and *36b4*, using the Livak ($2^{-\Delta\Delta Ct}$) method. Samples were run on a Quantstudio 6 flex Real-Time PCR System (RRID:SCR_020239, Applied Biosystems).

2.5 | Hormone assay

Plasma concentrations of estradiol, testosterone, androstenedione, and progesterone were analyzed via sensitive isotope-dilution TurboFlow-LC-MS/MS methods for simultaneous quantification of estrogens[35] and androgens/corticosteroids.[36] These methods were developed for human serum and used without modifications in mice as described previously.[37] Samples were analyzed in six batches, each including standards for calibration curves, a blank, three un-spiked serum pool samples, three pooled controls spiked in low concentration, and three pooled controls spiked in high concentration. The matrix for control material was pooled human serum from prepubertal children and adults. The intra-day variation (CV %) of estradiol, testosterone, androstenedione, and progesterone in control material were ≤8.2%, ≤2.3%, ≤2.2% and ≤4.2%, respectively, and thereby within internal ordinary inter-day variation for batches including human patient samples. Detection limits (LOD) for the steroids were 4.04 pmol/L (estradiol), 0.012 nmol/L (testosterone), 0.042 nmol/L (androstenedione), and 0.036 nmol/L (progesterone), where the same control material was used.

2.6 | Dual-energy X-ray absorptiometry (DEXA)

Femora were scanned using a desktop dual-energy X-ray absorptiometry (DEXA) scanner (Saber XL, Norland Stratec) at a pixel size of 0.1 mm × 0.1 mm and a velocity 3.0 m/s.[38] The bone mineral density (BMD) was determined using the software supplied with the scanner. Quality control was performed by scans of two solid-state phantoms.

2.7 | Sperm count and motility

Sperm was obtained from cauda of snap-frozen epididymis in 1 ml PBS. Samples were centrifuged at 300 ***g*** for 15 min, and the supernatant was resuspended to a total volume of 150 µl. Samples were diluted to achieve a sperm count of between 10 and 200 spermatozoa in a total of 16 squares of a Bürker-Türk counting chamber (Thermo Fisher Scientific). To avoid evaporation, the counting chamber was left for 5 min in a moist chamber. The heads of spermatozoa were counted in a total of 64 squares and concentration was calculated by the following equation: (average spermatozoa counted/dilution factor)/squares counted (64). To retrieve live sperm, cauda epididymis was excised and placed in 400 µl Krebs-Ringer buffer. Five small incisions were made to

mince the tissue and allow the sperm to be separated from the tissue. The material was incubated for 30 min, at 37°C, 5% CO_2. Sperm was carefully resuspended in 100 µl Krebs-Ringer buffer and 10 µl was taken to determine the percentage of motile sperm by counting 200 cells in a phase contrast microscope by two independent investigators blinded to the genotype. Sperm motility was categorized as progressively motile (grade ab), non-progressively motile (grade c) and immotile (grade d) as recommended by WHO. Sperm morphology was assessed on Papanicolaou-stained smears and evaluated by two individual investigators blinded to the genotype.

2.8 | HE staining, immunohistochemistry, and evaluation

The IHC procedure and hematoxylin and eosin (HE) staining were performed as described previously.[39] In brief: Deparaffination and rehydration of 4 µm formaldehyde-fixed sections were accomplished with Tissue-Tek (RRID:SCR_020858, Sakura Finetek B.V.) and saturation in decreasing concentrations of ethanol. Some sections were stained with HE. Sections for IHC were demasked by microwave treatment for 1 min with full effect followed by 15 min at 50% effect, in citrate or TEG buffer. This was followed by incubation in 0.5% v/v H_2O_2 in water to block endogen peroxidase activity and incubation in 0.5% skimmed milk in TBS to block unspecific antibody binding. Primary antibodies (VASA (ab13840, RRID:AB_443012, 1:4000 TEG, Abcam), Vimentin (sc-373 717, RRID:AB_10917747, 1:5000 TEG, Santa Cruz), Erα (sc-542, RRID:AB_631470, 1:500 TEG, Santa Cruz), or CYP17A1 (ab134910, RRID_AB2895598, 1:500 citrate buffer, Abcam) were diluted in TBS and added to the sections overnight at 4°C, followed by 1 h incubation at room temperature. Secondary antibodies (ImmPRESS MP-7401 (RRID:AB_2336529) or MP-7402 (RRID:AB_2336528), Vector Laboratories) were added for 30 min at room temperature, followed by development with AEC (3-amino-9-cabazole, ImmPACT, SK-4205, RRID:AB_2336518, Vector Laboratories) and counterstaining with Mayer's hematoxylin. All experiments were performed alongside control sections where the omission of the primary antibody was the only difference, and no staining was observed in these. The sections were scanned using a NanoZoomer 2.0HT (RRID:SCR_021658) and analyzed with the software NDPview version 2.6.24 (both from Hamamatsu Photonics). Two independent investigators, blinded for the genotype, evaluated the IHC slides and determined the stage of spermatogenesis. IHC staining was classified according to an arbitrary semi-quantitative reference scale based on the intensity of the staining and the proportion of cells stained as previously described:[40] +++, strong staining in nearly all cells; ++, moderate staining in the majority of cells; +, weak staining or a low percentage of cells stained; +/−, very weak staining in single cells; none, no positive cells detected.

2.9 | X-gal staining

Tissue from male *Adgra3*$^{lacZ/+}$ and control mice was fixed in 4% PFA at room temperature for 30 min, washed in PBS, and rinsed at room temperature for 1 h in X-gal rinse buffer (2 mM $MgCl_2$, 0.2% NP-40, 0.1% sodium deoxycholate in PBS). Then, tissue was incubated in X-gal staining solution (50 mg/ml 5-bromo-4-chloro-3-indolyl -β-D-galactopyranoside (PanReac AppliChem) in rinse buffer containing 5 mM potassium ferricyanide, 5 mM potassium ferrocyanide), for 14 h at 4°C, followed by a PBS rinse and post-fixation in 4% PFA overnight. The tissue was paraffin-embedded and sectioned for histological evaluation.

2.10 | von Kossa and Alizarin Red staining

Formalin-fixed sections were deparaffinized and rinsed in deionized water (diH_2O). In von Kossa experiments, sections were incubated with 1% silver nitrate (AppliChem) under ultraviolet light for 20 min. Sections were then rinsed in diH_2O, exposed to 5% sodium thiosulfate for 5 min, rinsed in diH_2O, and counterstained with Mayer's hematoxylin. Sections were then dehydrated through graded alcohol and xylene. Staining with 2% Alizarin Red solution (pH 4.1–4.3, Merck) for 5 min was likewise performed on deparaffinized sections. Sections were then dehydrated in acetone and acetone-xylene (1:1) and finally cleared in xylene. A human fetal bone was used as positive a control in both staining protocols.

2.11 | Blue dye injection

To visualize the passageways of the male distal reproductive tract, the vas deferens, bladder, seminal vesicles, coagulation glands and urethra were dissected and placed in a petri dish. Under a dissection microscope, Evans blue dye (0.05% in 1 × PBS) was injected into the vas deferens using a blunt needle. The distribution of the blue dye was recorded, and images were obtained with a digital camera. The corresponding seminal vesicle (without blue dye)

were fixed in 4.7% PFA and stained with HE staining for the presence of sperm.

2.12 | Quantification and statistical analysis

All analyses were performed using GraphPad Prism 9 (RRID:SCR_002798, GraphPad Software, Inc.). We used parametric or non-parametric tests accordingly as specified in each analysis. Residuals were evaluated to validate the use of parametric tests with or without logarithmic transformation. For multiple-comparison correction, *post hoc* testing was done using Šídák correction, as indicated in each analysis. All plots with error bars are reported as mean ± SEM, and statistical significance was defined as $p \leq .05$.

3 | RESULTS

3.1 | Frequent infertility in *Adgra3*$^{-/-}$ mice despite normal epididymal sperm count

To investigate the reproductive role of ADGRA3, a global-*Adgra3* deficient mouse (denoted *Adgra3*$^{-/-}$) was generated. Littermates with an intact *Adgra3* gene were used as controls (*Adgra3*$^{+/+}$). *Adgra3*$^{-/-}$ or *Adgra3*$^{+/+}$ males were paired for 10 sequential breedings with 10 C57BL6/J females over 8 months (Figure 1B). Surprisingly, 55% (11 of 20) of the *Adgra3*$^{-/-}$ males were unable to produce offspring during the study period, while the remaining 45% (9 of 20) were fertile (Figure 1B). Among *Adgra3*$^{+/+}$ mice, 93% (14 of 15) were fertile during the study period (Figure 1B). The infertile males exhibited normal mounting behavior with no significant difference in plugging latency of the females (Figure 1C). Moreover, there was no difference in litter size for the fertile *Adgra3*$^{-/-}$ males compared with *Adgra3*$^{+/+}$ males (7.1 ± 0.4 vs. 7.2 ± 0.5 pups/litter, Figure 1D). Extraction of sperm from the cauda of the epididymis at of 8, 15 weeks, and 1-year-old mice showed similar sperm concentrations in control and knockout mice (33.9 ± 11.8 vs. 32.0 ± 7.9 × 10^6/ml; 55.1 ± 11.9 vs. 54.5 ± 6.9 × 10^6/ml; and 25.1 ± 2.3 vs. 12.4 ± 8.6 × 10^6/ml, respectively, Figure 1E). When subdividing the *Adgra3*$^{-/-}$ males according to fertility, the sperm count in the infertile males did not differ from *Adgra3*$^{+/+}$ mice (Figure 1E). At 8 weeks of age, sperm of progressive motility (30.4 ± 5.5 vs. 30.8 ± 11.2) and sperm morphology did not differ between *Adgra3*$^{-/-}$ and *Adgra3*$^{+/+}$ littermates (Figure 1F and Figure S1A).

ADGRA3 has two similar sub-group members; ADGRA1 (GPR123) and ADGRA2 (GPR124).[17,18] When examining the expression pattern of the sub-group within the urogenital system of male C57BL/6J mice, we observed *Adgra3* and *Adgra2* expression within almost all tissues (Figure 1G and Figure S1B). However, in contrast to *Adgra3*, *Adgra2* was not expressed in the testis, and *Adgra1* was only expressed in Tyson's gland and the pituitary gland (Figure 1G and Figure S1B,C). The highest expression of *Adgra3* was in the kidney, and to a lower extent, in the testis and epididymis (30.2% and 16.5% of *Adgra3* expression in the kidney, respectively, Figure 1G). We used a LacZ mouse model (*Adgra3*$^{lacZ/+}$)[26,29,30] to visualize the expression pattern. *Adgra3* expression was present within both the epididymis, through the efferent tubules and into the testis (Figure 1H) and was confirmed in the edge of the seminiferous tubules (Figure 1I).[25,26,41] Furthermore, *Adgra3* expression was also detected in the renal cortex (Figure 1J).

3.2 | Abnormal testicular histology in *Adgra3*$^{-/-}$ mice

To further investigate the reproductive phenotype of the *Adgra3*$^{-/-}$ mice, we measured testicular weight in mice aged 8, 15 weeks, and 1 year, which were similar in *Adgra3*$^{-/-}$ and control mice (Figure 2A). Thorough histological analysis showed that 71% (5 of 7) of the 8-week-old *Adgra3*$^{-/-}$ mice had seminiferous tubules with secondary germinal epithelial degeneration, as evidenced by tubular vacuolation, segmental depletion of germ cells, and disordered arrangement of germ cell layers (Figure 2B and Figure S2A). None of the aged-matched *Adgra3*$^{+/+}$ mice exhibited this pathology. At 15 weeks, germinal epithelial degeneration was observed in 75% (6 of 8) of the *Adgra3*$^{-/-}$ males, and in 13% (1 of 8) of the control mice (Figure 2B). At 1 year, 85% (6 of 7) *Adgra3*$^{-/-}$ males showed germinal epithelial degeneration, with 29% (2 of 7) progressing to end-stage lesion of germinal epithelial atrophy throughout most of the testis (Figure 2B and Figure S2B). No mice in the 1-year-old control cohort exhibited degenerated or atrophied epithelia. Several mice with germinal epithelial degeneration had multinucleated giant cells (Figure 2B), a phenomenon resulting from incomplete cytogenesis,[42] as well as sperm stasis and hyalinization (Figure S2B). We further observed dystrophic microcalcification due to hydroxyapatite deposition within the seminiferous tubules in 29% (2 of 7) of the 1-year-old *Adgra3*$^{-/-}$ mice, verified by von Kossa and Alizarin Red staining (Figure 2C). Cell composition within the seminiferous tubules was evaluated by IHC markers for germ cells (VASA), Sertoli cells (vimentin), and Leydig cells (CYP17A1), which

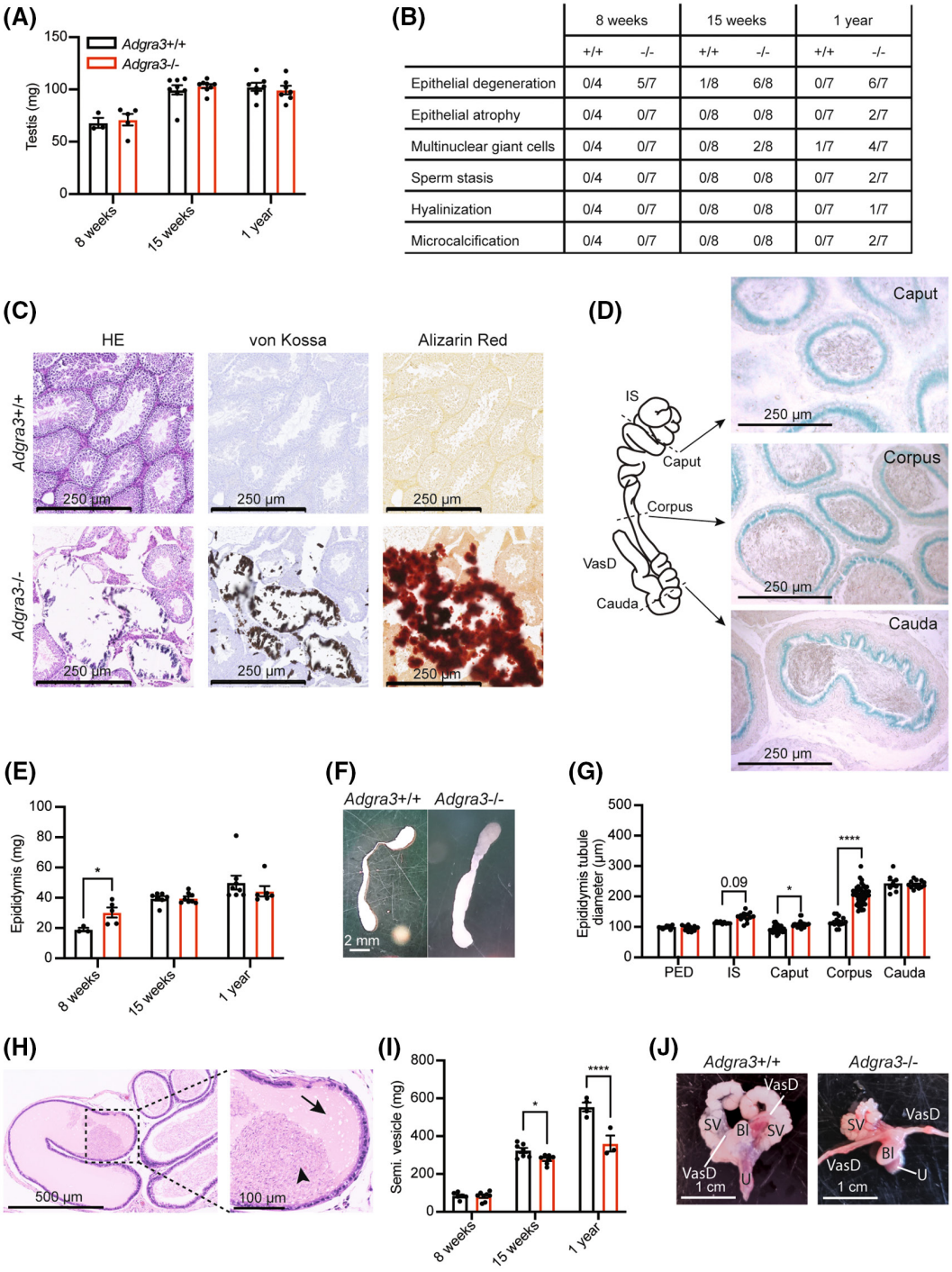

	8 weeks		15 weeks		1 year	
	+/+	-/-	+/+	-/-	+/+	-/-
Epithelial degeneration	0/4	5/7	1/8	6/8	0/7	6/7
Epithelial atrophy	0/4	0/7	0/8	0/8	0/7	2/7
Multinuclear giant cells	0/4	0/7	0/8	2/8	1/7	4/7
Sperm stasis	0/4	0/7	0/8	0/8	0/7	2/7
Hyalinization	0/4	0/7	0/8	0/8	0/7	1/7
Microcalcification	0/4	0/7	0/8	0/8	0/7	2/7

FIGURE 2 Testicular histopathology and enlargement of the epididymal ducts in *Adgra3*$^{-/-}$ mice. (A) Testicular weight of *Adgra3*$^{-/-}$ mice and littermate controls at 8, 15 weeks, and 1 year of age ($n = 5–8$). (B) Histopathological evaluation of testis by hematoxylin and eosin (HE) staining at all three age groups ($n = 4–8$). (C) Microcalcification in *Adgra3*$^{+/+}$ and *Adgra3*$^{-/-}$ mice as visualized by staining with either HE, von Kossa, or Alizarin red. (D) Right; Illustration of segments of epididymis, divided into initial segment (IS), caput, corpus, cauda, and vas deferens (VasD). Left; Representative pictures of X-gal-stained epididymis from *Adgra3*$^{lacZ/+}$ mice. (E) Weight of epididymis of *Adgra3*$^{-/-}$ and control mice at ages 8, 15 weeks, and 1 year ($n = 5–8$). (F) Representative pictures of epididymis dissected from 8-week-old *Adgra3*$^{+/+}$ and *Adgra3*$^{-/-}$ mice. (G) Epididymal duct diameter in 8-week-old mice, subdivided into five regions of epididymis; proximal efferent ducts (PED), IS, caput, corpus, and cauda. (H) HE staining of the transition between corpus and cauda of the epididymis in an 8-week-old *Adgra3*$^{-/-}$ mouse. Magnified inset shows hyalinization (arrow) and sperm stasis (arrowhead) within the dilated duct. (I) Seminal vesicle weight of *Adgra3*$^{-/-}$ mice and littermate controls at age 8, 15 weeks, and 1 year of age ($n = 3–8$). (J) Pictures of seminal vesicles of *Adgra3*$^{+/+}$ (left) and *Adgra3*$^{-/-}$ mice (right) of 15-weeks-old mice. The *Adgra3*$^{-/-}$ seminal vesicle is lacking the right seminal gland. SV, seminal vesicle; Bl, bladder; VasD, vas deferens; U, urethra. Data are presented as mean ± SEM. Comparisons were made using two-way ANOVA with Šídák correction for multiple comparisons. *$p < .05$, ****$p < .0001$.

showed no difference in expression between genotypes (Figure S2C–E).

3.3 | Dilated and enlarged epididymis in *Adgra3*$^{-/-}$ mice

Consistent with *Adgra3* mRNA expression in the epididymis of male mice (Figure 1G), the *Adgra3*$^{lacZ/+}$ mouse model confirmed the presence of ADGRA3 within the entire epithelium, in caput, corpus, and cauda (Figure 2D). Comparison of 8-week-old mice revealed a 1.6-fold higher epididymal weight in *Adgra3*$^{-/-}$ mice (19.0 ± 1.2 vs. 30.3 ± 3.3 mg, $p = .046$) (Figure 2E,F). This was accompanied by a dilation of the epididymal ducts across the caput and corpus of the epididymis (92.7 ± 2.3 vs. 107.4 ± 1.9 µm, $p = .025$ and 116.5 ± 3.9 vs. 205.9 ± 4.5 µm, $p < .0001$, respectively), but not in the efferent ducts or initial segment of the epididymis (Figure 2G and Figure S2F), which both are highly sensitive to fluid/electrolyte balance.[12] Interestingly, at the transition between corpus and cauda epididymis, we observed hyalinization (Figure 2H, arrow) and sperm stasis (Figure 2H, arrowhead) in 14% (1 of 7) of 8-week-old *Adgra3*$^{-/-}$ mice. The epididymal epithelia appeared morphologically normal and no obvious differences in epididymal sperm content could be seen in any of the remaining animals across genotype and age. At 1 year of age, there were no difference in epididymal weight or luminal diameter between genotypes (Figure 2E and Figure S2G). For reference, the diameter of the seminiferous tubules did not differ (Figure S2H), and the rete testis area did not look obviously different between *Adgra3*$^{-/-}$ and control mice. Although the weight of the seminal vesicles was similar across genotypes at 8 weeks of age, where at 15 weeks and 1 year of age the seminal vesicles of *Adgra3*$^{-/-}$ mice weighed substantially less than those of control mice (277.2 ± 9 vs. 324.4 ± 13 mg, $p = .045$ and 361.0 ± 42 vs. 554.5 ± 23 mg, $p < .0001$, respectively, Figure 2I). One 1-year-old *Adgra3*$^{-/-}$ mouse was even lacking a seminal gland while that of the other part of the gland remained markedly underdeveloped on visual inspection (Figure 2J).

3.4 | Altered estradiol production and signaling

The phenotypic effects on both epididymis and seminal vesicle suggest a possible disturbance of the endocrine system, but no significant differences in plasma concentrations of testosterone, androstenedione, or progesterone were detected in 15-week-old animals (Figure 3A–C). However,

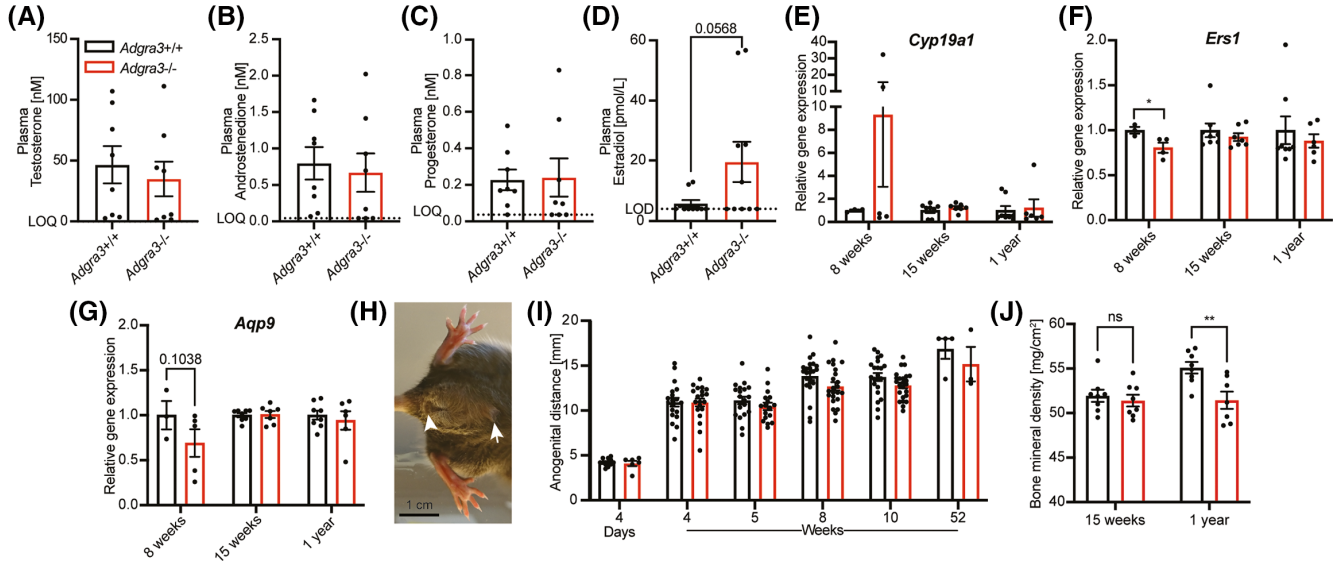

FIGURE 3 Lack of *Adgra3* causes altered plasma estradiol, estrogen-associated gene expression and decreased bone mineral density. (A–D) Plasma testosterone (A), androstenedione (B), progesterone (C), and estradiol (D) measured by LC-MS/MS on 15-weeks old *Adgra3*$^{-/-}$ mice and littermate controls. Limit of quantification (LOQ) and limit of detection (LOD) determined in human serum[35,36] ($n = 8$). (E–G) mRNA expression levels of aromatase (*Cyp19a1*) (E), estrogen receptor α (*Esr1*) (F), and aquaporin-9 (*Aqp9*) (G) at 8, 15 weeks and 1 year of age ($n = 4$–8). (H) Representative photograph of a male *Adgra3*$^{+/+}$ mouse showing anogenital distance (AGD) as measured between the rectum (white arrowhead) and penis (white arrow). (I) AGD measured at 4 days, 4-, 5-, 8-,10-, and 52-week-old in *Adgra3*$^{-/-}$ mice and littermate controls males ($n = 3$–24). (J) Bone mineral density (BMD) of the right femur of 15-week-old and 1-year-old animals ($n = 7$–8). In all datasets, each dot represents a single animal. Data presented as mean ± SEM. Statistics include a two-tailed Student's *t* test (A–D), and two-way ANOVA with Šídák correction for multiple comparisons (E–G, I,J). *$p < .05$, **$p < .01$.

Adgra3$^{-/-}$ mice had on average a 3-fold higher estradiol concentration than their *Adgra3*$^{+/+}$ littermates (19.6 ± 6.7 vs. 5.9 ± 1.1 pmol/L, $p = .057$, Figure 3D). However, this difference did not reach the level of significance, likely due to estradiol concentration being below the detection level (LOD) in some *Adgra3*$^{+/+}$ samples ($n = 7$ of 10), and the high variability of plasma sex steroid levels. In accordance with the numerically higher estradiol levels, 8-week-old *Adgra3*$^{-/-}$ mice had higher testicular expression of aromatase (*Cyp19a1*), the enzyme responsible for estradiol synthesis, than their littermate controls (Figure 3E). In contrast, expression of estrogen receptor 1 (*Esr1*) was reduced and expression of its downstream effector protein aquaporin-9 (*Aqp9*) was lower in 8-week-old *Adgra3*$^{-/-}$ testis compared to controls (Figure 3F,G). Expression of other factors involved in fluid reabsorption, such as *Cftr*, *Nhe3*, *CaII*, *CaIV*, *CaXIV*, and *Aqp1* remained similar across genotype in testis (Figure S3A–E), and expression of *Cftr*, *Nhe3*, *CaII*, and *CaIV* was similar in epididymis (Figure S3I–L) and vas deferens (Figure S3O–R) across genotype. Furthermore, ERα expression was unaltered in the testis (Figure S2C–E).

To evaluate adequate fetal androgen exposure, we measured AGD at multiple ages (Figure 3H), and found that in keeping with unaltered androgen levels, no significant difference was detected between genotypes (Figure 3I). Likewise, androgen receptor (*Ar*) and anti-Müllerian hormone receptor 2 (*Amhr2*) expression was unchanged between genotypes at all ages (Figure S3F,G). So did other sex hormone receptors in both testis, epididymis, and vas deferens (Figure S3H,M,N,S,T).

Like female mice, plasma estradiol fluctuates in male mice, but persistent estradiol deficiency may lower bone mineral density (BMD).[43] Therefore, BMD of the femora of 15-week-old and 1-year-old mice was measured. At 15 weeks, BMD did not differ between *Adgra3*$^{-/-}$ and control mice. However, with increasing age the difference became apparent, and at 1 year the *Adgra3*$^{-/-}$ mice had significantly lower BMD than the control mice (0.055 vs. 0.051 g/cm^2, $p = .0037$, Figure 3J).

3.5 | Obstruction at the junctions of vas deferens and urethra causes infertility

To investigate the physiological cause of infertility in our models, blue dye was injected into the vas deferens to visualize the passage from vas deferens to the urethra (Figure 4A). In *Adgra3*$^{+/+}$ ($n = 13$) and fertile *Adgra3*$^{-/-}$ ($n = 7$) male mice, the dye traveled unhindered through the vas deferens to the bladder and urethra but bypassed the seminal vesicle (Figure 4B,C). However, in infertile *Adgra3*$^{-/-}$ ($n = 6$) males, the dye did not pass into the bladder and urethra, but instead accumulated in the seminal vesicle (Figure 4D), which in one case was only half developed (Figure 2J). Histology of the seminal vesicle showed sperm accumulation in the infertile males (Figure 4G, arrowheads), but not in the fertile males (Figure 4E,F). Thus, the infertile *Adgra3*$^{-/-}$ mice had an obstruction in the distal part of the male reproductive tract.

4 | DISCUSSION

In the present study, half of the mice lacking *Adgra3* were infertile due to obstructive azoospermia, resulting from effects on the epithelial lining of the male reproductive and the accessory organs rather than a direct testicular phenotype. ADGRA3 has been reported as a spermatogonial stem cell marker,[25,26,41] and our data support its expression in spermatogonia as ADGRA3. In line with a previous study showing spermatogonial stem cells maintaining progenitor stem cell properties despite deletion of the cytoplasmic domain of *Adgra3*,[26] we found no major change in germ cell numbers, spermatogenesis, sperm count, motility or morphology following loss of *Adgra3*. Thus, ADGRA3 is not required for normal spermatogenesis. However, we found a distal reproductive tract obstruction in the *Adgra3*$^{-/-}$ males causing sperm and fluid accumulation within the epididymis. The seminal vesicles of these mice were smaller and had abnormal structure or were absent entirely, a similar phenotype observed in mice expressing a point mutation in β-catenin, C429S.[44] These findings suggest defective development or maintenance of the caudal Wolffian ducts in the mice lacking ADGRA3 and support the notion that ADGRA3 signals through the WNT/β-catenin pathway.[33]

Early during male development, the vas deferens and seminal vesicle ducts fuse to form the ejaculatory duct, which joins with urogenital sinus-originating tissue.[45] Based on the dye accumulation in the seminal vesicles, the fusion of the ejaculatory duct with the urogenital sinus has failed in infertile *Adgra3*$^{-/-}$ mice. Therefore, ADGRA3 may also play a role in mechanotransduction and migration when the tip of the ejaculatory duct reaches the urogenital sinus, as *Adgra3*-positive cells are present in the tip of other migrating embryonic duct systems.[29,30] This finding is novel, as androgens have been considered the primary regulator of Wolffian duct development in conjunction with other growth factors, that is, TGFβ, FGF3, and IGF1.[46] In accordance, we find unaltered plasma testosterone levels in *Adgra3*$^{-/-}$ mice, indicating that the phenotype observed is a direct consequence of *Adgra3* deficiency, or possibly affected by downstream signaling via endocrine or paracrine factors, such as, estradiol.

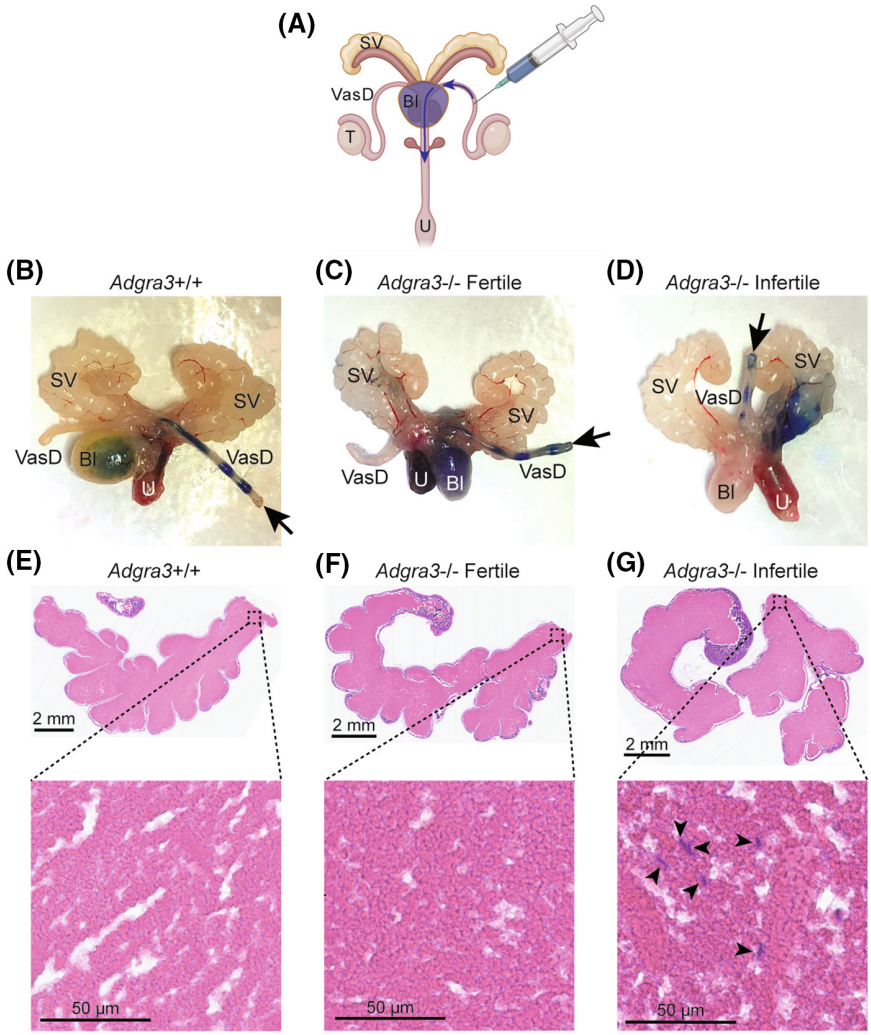

FIGURE 4 Obstruction in the distal reproductive tract causes sperm trapped in the seminal vesicles. (A) Blue dye was injected into the vas deferens to visualize passage or blockage to the urethra at 15 weeks of age. (B–D) Representative photographs of reproductive organs dissected from 15-week-old fertile *Adgra3*$^{+/+}$ ($n = 13$) (B), fertile *Adgra3*$^{-/-}$ ($n = 7$) (C), and infertile *Adgra3*$^{-/-}$ ($n = 6$) mice (D) showing vas deferens (VasD), seminal vesicle (SV), bladder (Bl), and urethra (U) after injection with blue dye. Arrows indicate injection site of dye into vas deferens. (E–G) Upper panel: HE staining of seminal vesicles dissected from 15-week-old fertile *Adgra3*$^{+/+}$ (E), fertile *Adgra3*$^{-/-}$ (F), and infertile *Adgra3*$^{-/-}$ (G) mice. Lower panel: Magnified inset showing tissue with arrowheads indicating heads of spermatozoa present. (A) was created with Biorender.com.

Estradiol is synthesized at high levels in the testis and plays a vital role in the development of the male reproductive system.[9] Eight-week-old *Adgra3*$^{-/-}$ mice had increased aromatase (*Cyp19a1*) expression and elevated plasma estradiol, which could represent a compensatory response to the observed reduction in the main estrogen receptor expression. On the other hand, the increased estradiol did not decrease *Ar* expression, as reported previously,[47] which suggests that loss of *Adgra3* may lead to uncoupling of the relationship between estrogen and androgen receptor expression. *Esr1* is crucial for fluid handling in the male reproductive tract, and mice lacking the *Esr1* gene exhibit dilatation of the epididymis[12] and decreased aquaporin-9 (*Aqp9*) expression. Aquaporin-9 in turn controls fluid reabsorption in the efferent duct and epididymis, and its expression is regulated by ERα and the androgen receptor.[10,11] *Adgra3* is also found to be expressed within the efferent ducts and epididymis. Epididymal dilation was only observed in 8-week-old *Adgra3*$^{-/-}$ mice and was not seen in the 15-week-old or 1-year-old cohorts, implying that the phenotype is reversible and/or compensated later in life. The early phenotype implies that there could be a link between ERα and ADGRA3 that regulates the WNT/β-catenin pathways,[32,33,48–50] and that in adult life this effect can be compensated. Alternatively, sex steroids, such as estradiol, could bind directly to ADGRA3, as shown recently by testosterone binding to ADGRG1, formerly GPR56.[51] The severe phenotype in half of the mice and mild testicular phenotype in the remaining with loss of ADGRA3 indicate that there is a distal effect, which is fully compensated in half of the males and prevents obstruction, while all have a mild testis or efferent duct effect that results in epithelial degeneration.

ADGRG1 is expressed in Sertoli cells, and loss of function results in abnormal formation of seminiferous tubules during embryogenesis and infertility.[22] ADGRG2 (GPR64) is highly expressed in the apical compartment of nonciliated principal cells of the rete testis and the proximal epididymis[52,53] and is responsible for absorption of testicular fluids within the epididymis to concentrate sperm.[23] Mutations in the human ADGRG2 gene cause congenital bilateral absence of vas deferens (CBAVD) and male infertility,[20] and male *Adgra2*-knockout mice display fluid dysregulation and spermatozoa obstruction in the efferent

ductules.[52,54] Combined with our novel findings linking ADGRA3 to obstructive azoospermia, this indicates that drugs targeting these aGPCRs may be used as future therapeutics to modulate male reproductive function.

Obstructive azoospermia is defined as the absence of spermatozoa in the ejaculate despite normal spermatogenesis and is identified in approximately 1% of all men and in 6%–14% of infertile men.[55,56] Ejaculatory duct obstruction is a rare cause of obstructive azoospermia. As in our *Adgra3*$^{-/-}$ mice, men with ejaculatory duct obstruction have normal testicular volume and fully developed vas deferens.[56] The seminal vesicles are mostly unremarkable in these men but may be enlarged or have a midline nodule in the prostate.[56] In the mouse model, we see a smaller seminal vesicle at an advanced age, possibly as a direct effect of *Adgra3*-deficiency rather than through altered estradiol production or signaling. Lastly, patients with ejaculatory duct obstruction have normal gonadotropin and testosterone concentrations, but ultrasonography frequently show calcification within the ejaculatory duct, prostate, or testis.[56] All of this is consistent with what we observe in our mouse model. This supports the inclusion of ADGRA3 in the genetic evaluation of male infertility, particularly obstructive azoospermia.

In conclusion, we studied the function of ADGRA3 in male mice. We found that the ejaculatory duct of *Adgra3*-deficient mice fails to reach the urogenital sinus during early development, resulting in the same ejaculatory duct obstruction phenotype observed in men suffering from obstructive infertility. The clinical link between ADGRA3 and male infertility requires further investigation to determine potential therapeutic applications further.

AUTHOR CONTRIBUTIONS

The study was conceptualized by Mette M. Rosenkilde and Maja L. Nybo, and the main investigation was performed by Maja L. Nybo and Jone M. Kvam. John E. Nielsen performed the histological experiments, while Maja L. Nybo, Jone M. Kvam, and Martin Blomberg Jensen did the histological examinations. The *Adgra3*$^{lacZ/+}$ mouse was generated at Pamela Cowin's laboratory, where Kristian H. R. Jensen fixed and stained the tissue from these mice. Hanne Frederiksen and Anders Juul analyzed and interpreted the hormone data. Sarina Gadgaard and Jesper S. Thomsen analyzed and interpreted the bone density data. Katja Spiess generated the *Adgra3*$^{-/+}$ mice. Maja L. Nybo, Mette M. Rosenkilde, and Martin Blomberg Jensen wrote the original draft, and all authors revised and approved the final manuscript.

ACKNOWLEDGMENTS

The authors thank Ana Ricci Nielsen for technical assistance in immunohistochemistry.

FUNDING INFORMATION

The project was funded by the European Research Council, ERC, (CoG, 682549), the Lundbeck Foundation (R268-2017-409), the Novo Nordisk Foundation (NNF17OC0029222), a donation from deceased Valter Alex Torbjørn Eichmuller (2020-117043) and the Kirsten and Freddy Johansens Foundation (KFJ, 2017-112697) for M.M.R.; the Novo Nordisk Foundation (NNF20OC0059475) and Dansk Frie Forskningsråd for M.B.J.; Department of Defense (W81XWH-17-1-0013 BC160959) to P.C.

DISCLOSURES

The authors declare no conflicts of interest.

DATA AVAILABILITY STATEMENT

The datasets used and/or analyzed during the current study are available from the corresponding author on reasonable request. Mouse lines generated in this study will be shared upon request after completion of Material Transfer Agreement due to institutional policy and will be deposited to a mouse repository.

ETHICS APPROVAL AND CONSENT TO PARTICIPATE

Mice housing and experiments were conducted according to institutional guidelines and approved by the Animal Experiments Inspectorate under the Danish Ministry of Food, Agriculture, and Fisheries (license numbers 2018-15-0201-01442, 2017-15-0202-00117 and 2017-15-0201-01235).

CONSENT FOR PUBLICATION

Not applicable.

REFERENCES

1. Boivin J, Bunting L, Collins JA, Nygren KG. International estimates of infertility prevalence and treatment-seeking: potential need and demand for infertility medical care. *Hum Reprod*. 2007;22(6):1506-1512.
2. Lunenfeld B. Infertility in the third millennium: implications for the individual, family and society: condensed meeting report from the Bertarelli Foundation's second global conference. *Hum Reprod Update*. 2004;10(4):317-326.
3. Hamada AJ, Montgomery B, Agarwal A. Male infertility: a critical review of pharmacologic management. *Expert Opin Pharmacother*. 2012;13(17):2511-2531.
4. Jodar M, Sendler E, Moskovtsev SI, et al. Absence of sperm RNA elements correlates with idiopathic male infertility. *Sci Transl Med*. 2015;7(295):295re6.
5. Skakkebaek NE, Rajpert-De Meyts E, Buck Louis GM, et al. Male reproductive disorders and fertility trends: influences of environment and genetic susceptibility. *Physiol Rev*. 2016;96(1):55-97.

6. Oatley JM, Brinster RL. Regulation of spermatogonial stem cell self-renewal in mammals. *Annu Rev Cell Dev Biol*. 2008;24:263-286.
7. Holstein AF. E. Knobil, J. D. Neill (eds): The physiology of reproduction. *Andrologia*. 2009;26(6):357.
8. Oduwole OO, Peltoketo H, Huhtaniemi IT. Role of follicle-stimulating hormone in spermatogenesis. *Front Endocrinol*. 2018;9:763.
9. Hess RA, Sharpe RM, Hinton BT. Estrogens and development of the rete testis, efferent ductules, epididymis and vas deferens. *Differentiation*. 2021;118:41-71.
10. Pastor-Soler N, Isnard-Bagnis C, Herak-Kramberger C, et al. Expression of aquaporin 9 in the adult rat Epididymal epithelium is modulated by androgens. *Biol Reprod*. 2002;66(6):1716-1722.
11. Oliveira CA, Carnes K, França LR, Hermo L, Hess RA. Aquaporin-1 and −9 are differentially regulated by oestrogen in the efferent ductule epithelium and initial segment of the epididymis. *Biol Cell*. 2005;97(6):385-395.
12. Hess RA, Bunick D, Lee K-H, et al. A role for oestrogens in the male reproductive system. *Nature*. 1997;390(6659):509-512.
13. Fredriksson R, Lagerström MC, Lundin L-G, Schiöth HB. The G-protein-coupled receptors in the human genome form five Main families. Phylogenetic analysis, paralogon groups, and fingerprints. *Mol Pharmacol*. 2003;63(6):1256-1272.
14. Hamann J, Aust G, Araç D, et al. International Union of Basic and Clinical Pharmacology. XCIV. Adhesion G protein–coupled receptors. *Pharmacol Rev*. 2015;67(2):338-367.
15. Yates LL, Papakrivopoulou J, Long DA, et al. The planar cell polarity gene Vangl2 is required for mammalian kidney-branching morphogenesis and glomerular maturation. *Hum Mol Genet*. 2010;19(23):4663-4676.
16. Patat O, Pagin A, Siegfried A, et al. Truncating mutations in the adhesion G protein-coupled receptor G2 gene ADGRG2 cause an X-linked congenital bilateral absence of vas deferens. *Am J Hum Genet*. 2016;99(2):437-442.
17. Haitina T, Olsson F, Stephansson O, et al. Expression profile of the entire family of AdhesionG protein-coupled receptors in mouse and rat. *BMC Neurosci*. 2008;9(1):43.
18. Chen G, Yang L, Begum S, Xu L. GPR56 is essential for testis development and male fertility in mice. *Dev Dyn*. 2010;239(12):3358-3367.
19. Kirchhoff C, Osterhoff C, Samalecos A. HE6/GPR64 adhesion receptor co-localizes with apical and subapical F-actin scaffold in male excurrent duct epithelia. *Reproduction*. 2008;136(2):235-245.
20. Mali P, Virtanen I, Parvinen M. Vimentin expression in spermatogenic and sertoli cells is stage-related in rat seminiferous epithelium. *Andrologia*. 2009;19(6):644-653.
21. Seandel M, James D, Shmelkov SV, et al. Generation of functional multipotent adult stem cells from GPR125+ germline progenitors. *Nature*. 2007;449(7160):346-350.
22. Seandel M, Falciatori I, Shmelkov SV, Kim J, James D, Rafii S. Niche players: spermatogonial progenitors marked by GPR125. *Cell Cycle*. 2008;7(2):135-140.
23. Guo Y, Hai Y, Gong Y, Li Z, He Z. Characterization, isolation, and culture of mouse and human spermatogonial stem cells: distinct characteristics between mouse and human SSCs. *J Cell Physiol*. 2014;229(4):407-413.
24. Pickering C, Hägglund M, Szmydynger-Chodobska J, et al. The adhesion GPCR GPR125 is specifically expressed in the choroid plexus and is upregulated following brain injury. *BMC Neurosci*. 2008;9(1):97.
25. Spina E, Handlin R, Simundza J, et al. Gpr125 identifies myoepithelial progenitors at tips of lacrimal ducts and is essential for tear film. *Dev Biol*. 2020. Preprint. http://biorxiv.org/lookup/doi/10.1101/2020.09.15.296749
26. Spiess K, Bagger SO, Torz LJ, et al. Arrestin-independent constitutive endocytosis of GPR125/ADGRA3. *Ann N Y Acad Sci*. 2019;1456(1):186-199.
27. Li X, Roszko I, Sepich DS, et al. Gpr125 modulates Dishevelled distribution and planar cell polarity signaling. *Development*. 2013;140(14):3028-3039.
28. Wu Y, Chen W, Gong L, Ke C, Wang H, Cai Y. Elevated G-protein receptor 125 (GPR125) expression predicts good outcomes in colorectal cancer and inhibits Wnt/β-catenin signaling pathway. *Med Sci Monit*. 2018;24:6608-6616.
29. Manno FAM. Measurement of the digit lengths and the anogenital distance in mice. *Physiol Behav*. 2008;93(1-2):364-368.
30. Frederiksen H, Johannsen TH, Andersen SE, et al. Sex-specific estrogen levels and reference intervals from infancy to late adulthood determined by LC-MS/MS. *J Clin Endocrinol Metab*. 2020;105(3):754-768.
31. Søeborg T, Frederiksen H, Johannsen TH, Andersson A-M, Juul A. Isotope-dilution TurboFlow-LC-MS/MS method for simultaneous quantification of ten steroid metabolites in serum. *Clin Chim Acta*. 2017;468:180-186.
32. Blomberg Jensen M, Andreassen CH, Jørgensen A, et al. RANKL regulates male reproductive function. *Nat Commun*. 2021;12(1):2450.
33. Boisen IM, Nielsen JE, Verlinden L, et al. Calcium transport in male reproduction is possibly influenced by vitamin D and CaSR. *J Endocrinol*. 2021;251(3):213-228.
34. Blomberg Jensen M, Lieben L, Nielsen JE, et al. Characterization of the testicular, epididymal and endocrine phenotypes in the Leuven Vdr-deficient mouse model: targeting estrogen signalling. *Mol Cell Endocrinol*. 2013;377(1-2):93-102.
35. Creasy D, Bube A, de Rijk E, et al. Proliferative and nonproliferative lesions of the rat and mouse male reproductive system. *Toxicol Pathol*. 2012;40(6_suppl):40S-121S.
36. Wolf C, Lambright C, Mann P, et al. Administration of potentially antiandrogenic pesticides (procymidone, linuron, iprodione, chlozolinate, p,p'-DDE, and ketoconazole) and toxic substances (dibutyl- and diethylhexyl phthalate, PCB 169, and ethane dimethane sulphonate) during sexual differentiation produces diverse profiles of reproductive malformations in the male rat. *Toxicol Ind Health*. 1999;15(1-2):94-118.
37. Welsh M, Saunders PTK, Fisken M, et al. Identification in rats of a programming window for reproductive tract masculinization, disruption of which leads to hypospadias and cryptorchidism. *J Clin Invest*. 2008;118(4):1479-1490.
38. Ettinger B. Associations between low levels of serum estradiol, bone density, and fractures among elderly women: the study of osteoporotic fractures. *J Clin Endocrinol Metab*. 1998;83(7):2239-2243.
39. Lin T-M. Region-specific inhibition of prostatic epithelial bud formation in the urogenital sinus of C57BL/6 mice exposed in utero to 2,3,7,8-tetrachlorodibenzo-p-dioxin. *Toxicol Sci*. 2003;76(1):171-181.

40. Georgas KM, Armstrong J, Keast JR, et al. An illustrated anatomical ontology of the developing mouse lower urogenital tract. *Development*. 2015;142(10):1893-1908.
41. Murata T, Ishitsuka Y, Karouji K, et al. β-cateninC429S mice exhibit sterility consequent to spatiotemporally sustained Wnt signalling in the internal genitalia. *Sci Rep*. 2015;4(1):6959.
42. Mehta V, Abler LL, Keil KP, Schmitz CT, Joshi PS, Vezina CM. Atlas of Wnt and R-spondin gene expression in the developing male mouse lower urogenital tract. *Dev Dyn*. 2011;240(11):2548-2560.
43. Mulligan WA, Wegner KA, Keil KP, Mehta V, Taketo MM, Vezina CM. Beta-catenin and estrogen signaling collaborate to drive cyclin D1 expression in developing mouse prostate. *Differentiation*. 2017;93:66-71.
44. Mehta V, Schmitz CT, Keil KP, et al. Beta-catenin (CTNNB1) induces bmp expression in urogenital sinus epithelium and participates in prostatic bud initiation and patterning. *Dev Biol*. 2013;376(2):125-135.
45. Hannema SE, Hughes IA. Regulation of Wolffian duct development. *Horm Res Paediatr*. 2007;67(3):142-151.
46. Hess RA, Bunick D, Lubahn DB, Zhou Q, Bouma J. Morphologic changes in efferent ductules and epididymis in estrogen receptor-alpha knockout mice. *J Androl*. 2000;21(1):107-121.
47. Ali M, Shahin SM, Sabri NA, Al-Hendy A, Yang Q. Activation of β-catenin signaling and its crosstalk with estrogen and histone deacetylases in human uterine fibroids. *J Clin Endocrinol Metab*. 2020;105(4):e1517-e1535.
48. Hou X, Tan Y, Li M, Dey SK, Das SK. Canonical Wnt signaling is critical to estrogen-mediated uterine growth. *Mol Endocrinol*. 2004;18(12):3035-3049.
49. Kasoha M, Dernektsi C, Seibold A, et al. Crosstalk of estrogen receptors and Wnt/β-catenin signaling in endometrial cancer. *J Cancer Res Clin Oncol*. 2020;146(2):315-327.
50. Singh JP, Dagar M, Dagar G, et al. Activation of GPR56, a novel adhesion GPCR, is necessary for nuclear androgen receptor signaling in prostate cells. *PLoS One*. 2020;15(9):e0226056.
51. Obermann H, Samalecos A, Osterhoff C, Schröder B, Heller R, Kirchhoff C. HE6, a two-subunit heptahelical receptor associated with apical membranes of efferent and epididymal duct epithelia. *Mol Reprod Dev*. 2003;64(1):13-26.
52. Osterhoff C, Ivell R, Kirchhoff C. Cloning of a human epididymis-specific mRNA, HE6, encoding a novel member of the seven transmembrane-domain receptor superfamily. *DNA Cell Biol*. 1997;16(4):379-389.
53. Davies B, Baumann C, Kirchhoff C, et al. Targeted deletion of the epididymal receptor HE6 results in fluid dysregulation and male infertility. *Mol Cell Biol*. 2004;24(19):8642-8648.
54. Aziz N, Agarwal A, Nallella KP, Thomas AJ Jr. Relationship between epidemiological features and aetiology of male infertility as diagnosed by a comprehensive infertility service provider. *Reprod Biomed Online*. 2006;12(2):209-214.
55. Jequier AM. Obstructive azoospermia: a study of 102 patients. *Clin Reprod Fertil*. 1985;3(1):21-36.
56. Baker K, Sabanegh E. Obstructive azoospermia: reconstructive techniques and results. *Clinics*. 2013;68(S1):61-73.

SUPPORTING INFORMATION

Additional supporting information can be found online in the Supporting Information section at the end of this article.

How to cite this article: Nybo ML, Kvam JM, Nielsen JE, et al. Loss of *Adgra3* causes obstructive azoospermia with high penetrance in male mice. *The FASEB Journal*. 2023;37:e22781. doi:10.1096/fj.202200762RR